Science Robotics

Supplementary Materials for
Soft wall-climbing robots

Guoying Gu,[1,2a]* Jiang Zou,[1a], Ruike Zhao,[3] Xuanhe Zhao,[3,4]* and Xiangyang Zhu,[1,2]*

[1]Robotics Institute, School of Mechanical Engineering, Shanghai Jiao Tong University, Shanghai 200240, China; [2]State Key Laboratory of Mechanical System and Vibration, Shanghai Jiao Tong University, Shanghai 200240, China; [3]Soft Active Materials Laboratory, Department of Mechanical Engineering, Massachusetts Institute of Technology, Cambridge, MA 02139, USA; [4]Department of Civil and Environmental Engineering, Massachusetts Institute of Technology, Cambridge, Massachusetts 02139, USA.

*To whom correspondence should be addressed. Email: guguoying@sjtu.edu.cn; zhaox@mit.edu; mexyzhu@sjtu.edu.cn

This file includes:

Text: description of the model simulation of the dielectric-elastomer actuator

Fig. S1. The structure design of the soft wall-climbing robot

Fig. S2. The fabrication process of the dielectric-elastomer actuator

Fig. S3. The assembly of the soft wall-climbing robot

Fig. S4. Model simulation of the dielectric-elastomer actuator

Fig. S5. Experimental setup for the electroadhesion measurement

Fig. S6. Experimental setup for the blocking force measurement

Fig. S7. Experimental setup for the extension measurement

Fig. S8. Maximum extension length calculated in one actuation cycle

Fig. S9. The surface topography of different substrates.

Table S1 The currently available soft crawling robots and soft climbing robots

Other Supplementary Material for this manuscript includes the following:

Movie S1 (.MP4 formant) Climbing experiments without payload

Movie S2 (.MP4 formant) Climbing experiments with a 10g payload

Movie S3 (.MP4 formant) Crawling experiments

Movie S4 (.MP4 formant) Turning experiments

Movie S5 (.MP4 formant) Video-recording while climbing a vertical tunnel

Movie S6 (.MP4 formant) Confined space navigation experiment

Movie S7 (.MP4 formant) Labyrinth trajectory tracking experiment

Movie S8 (.MP4 formant) Reciprocated crawl on the glass plane

Description of the model simulation of the dielectric-elastomer actuator

To account for the coupling of elastic and electromechanical deformation, we apply the existing model developed by Zhao et al. (*Applied Physics Letters* **93**, 251902, 2008). Taking the general neo-Hookean solid as the elastic representation of the dielectric-elastomer membrane (VHB 4910, undeformed thickness 1 mm), the free-energy function is defined as

$$W^{elastic} = \frac{\mu}{2}\left(F_{ij}F_{ij} - 3\right) + \frac{K}{2}(J-1)^2 - \frac{\varepsilon F_{ik}^{-1}E_k F_{il}^{-1}E_l}{2J} \tag{s1}$$

where μ , K and ε are the material's shear modulus, bulk modulus and electric permittivity, respectively, and $\mathbf{F}$ represents the deformation gradient tensor. The quantity J, the volumetric Jacobian of the deformation, is defined as $J = \det \mathbf{F}$.

The developed model in Eq. (s1) is further implemented through a user-defined material subroutine in the commercial finite element analysis (FEA) software ABAQUS. Here, the 10-node quadratic tetrahedron, hybrid element (C3D10H) is used to conduct the static simulation. In the simulation, we select $\mu = 0.2$ MPa as the initial shear modulus and the $\varepsilon_r = 4.5$ as the relevant dielectric constant for the dielectric-elastomer membrane in comparison to the experimental results. The nearly incompressible property of the dielectric-elastomer material is satisfied by setting the bulk modulus K to be much larger than the shear modulus μ ($K = 10^{10}\mu$).

1. Buckling simulation

In the reference state (with biaxial pre-stretch λ_{ps}, Fig. S4A-1), we assume the initial length between the actuator horizontal edges is L. In the un-actuated state (Fig. S4A-2), the dielectric-elastomer actuator buckles by releasing the pre-stretched dielectric elastomer and generates a contraction strain $\varepsilon_C = (L - L_C)/L$, where L_C is the buckled length between the actuator horizontal edges. Through FEA, we evaluate the critical λ_{ps} to reach certain contraction strain levels with different frame stiffness. Considering the geometry of the fabricated dielectric-elastomer actuator (Fig. S1), Fig. S4B shows the simulation results. We can see that the contraction strain linearly increases with the pre-stretch λ_{ps}. Based on this relationship, we measure the dielectric-elastomer actuator with the frame modulus E_f =4GPa and prestretch λ_{ps}=5, and the results (Fig. S4C and Fig. S4D) show good agreement between the model prediction and the experimental result with the contraction strain $\varepsilon_C = 0.21$.

2. Actuation simulation

In the current actuated state (Fig. S4A-3), when applying a voltage, the dielectric-elastomer actuator functions as the muscle and generates a corresponding strain $\varepsilon_A = (L_A - L_C)/L$, where L_A is the current length of the horizontal edge of the dielectric-elastomer actuator. Fig. S4E shows the corresponding actuation strain ε_A in terms of the applied electrical field E under different λ_{ps} for the dielectric-elastomer actuator with the constant modulus ratio $E_f / \mu = 0.5\times10^3$. We can see that relationships between ε_A and E is approximately linear when E is relatively small. However, with further increasing E, the maximum actuation strain is reached when the frame flattens completely (as indicated by dashed lines in Fig. S4E).

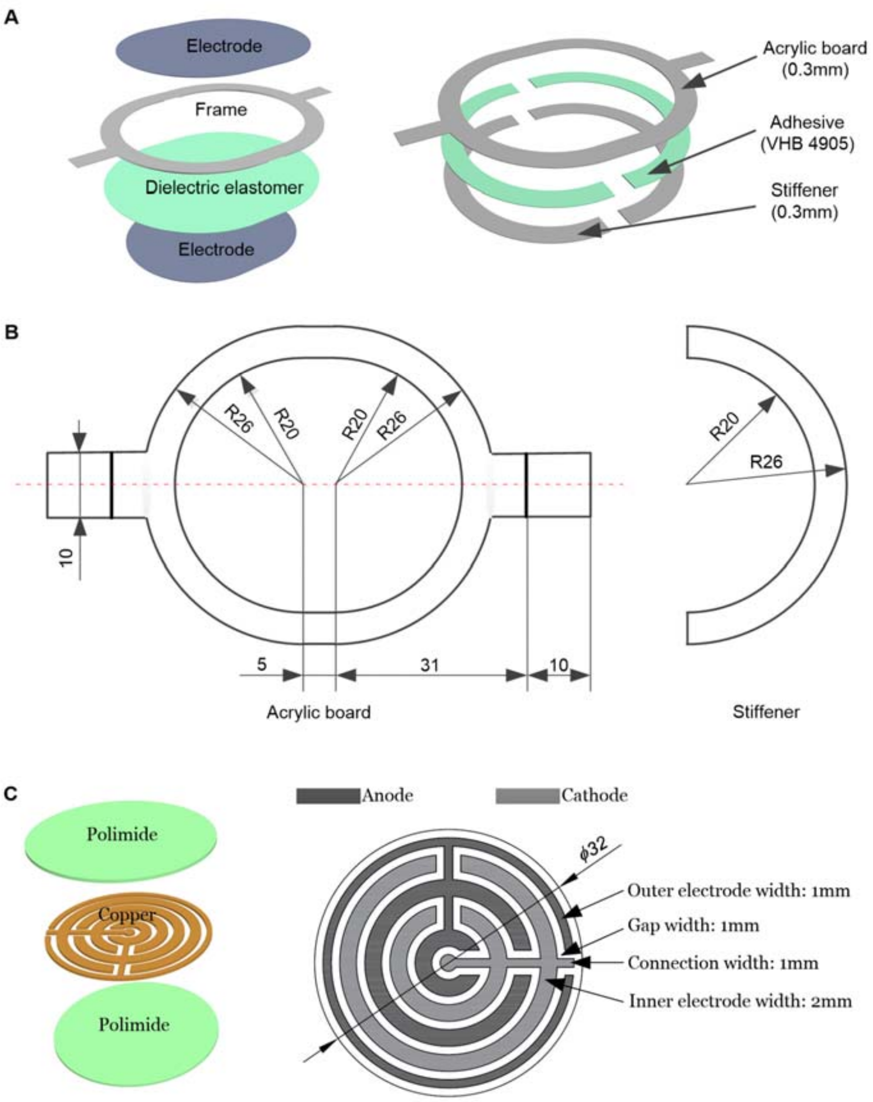

Fig. S1. The structure design of the soft wall-climbing robot. (A) The dielectric-elastomer actuator consists of a pre-stretched dielectric-elastomer membrane and a flexible acrylic frame. The dielectric-elastomer membrane (VHB 4910, undeformed thickness 1 mm) is biaxially pre-stretched by 5 times, sandwiched by two compliant carbon grease electrodes. The flexible acrylic frame is made of a laser cut acrylic board (thickness 0.3mm) and two stiffeners (thickness 0.3mm) adhered by a dielectric-elastomer adhesive (VHB 4905, thickness 0.5mm). **(B)** Geometry dimension of the acrylic board and the stiffener. **(C)** Geometry dimension of the electroadhesive foot made of copper (thickness 0.018mm) and two polyimide-membrane layers (thickness of each layer 0.02mm).

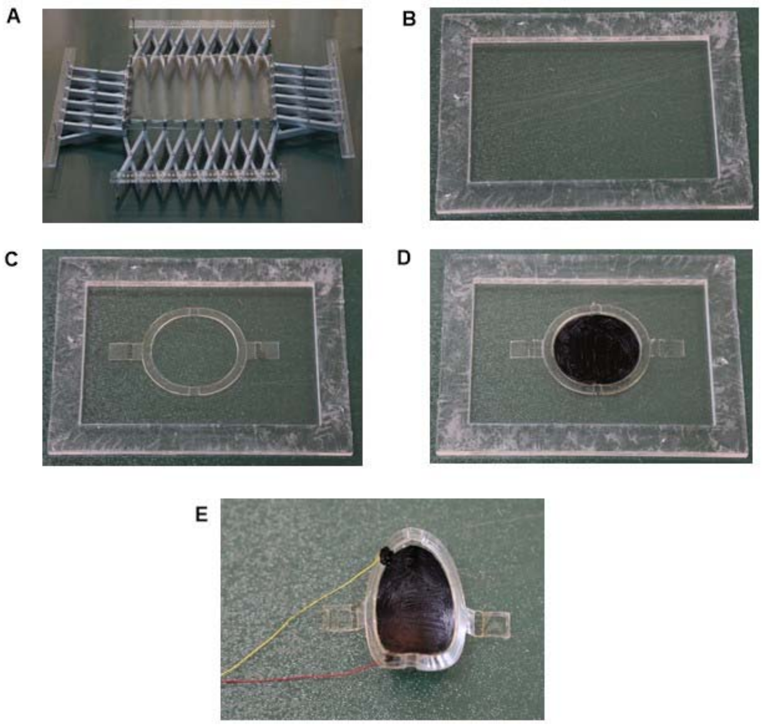

Fig. S2. The fabrication process of the dielectric-elastomer actuator. (A) Pre-stretching the dielectric-elastomer membrane with a stretcher with four fixtures. **(B)** Supporting the pre-stretched dielectric-elastomer membrane with a stiff acrylic frame (thickness, 5mm) (We kept the membrane for 12 hours to make it stable). **(C)** Stacking the flexible acrylic frame and membrane together. **(D)** Coating electrodes (carbon grease) on both sides of the membrane by a paintbrush. **(E)** Releasing the membrane to form a saddle-shape dielectric-elastomer actuator and connecting the electrodes to high voltage amplifier by soft wires (diameter, 0.35mm).

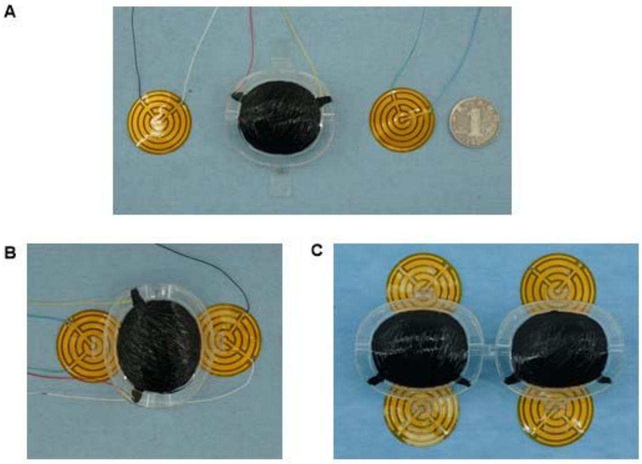

Fig. S3. The assembly of the soft wall-climbing robot. (A) Preparing a dielectric-elastomer actuator and two electroadhesive feet. **(B)** Assembling the dielectric-elastomer actuator and two electroadhesive feet to form a two-foot soft robot. **(C)** Scaling the two soft robots to build a four-foot soft robot.

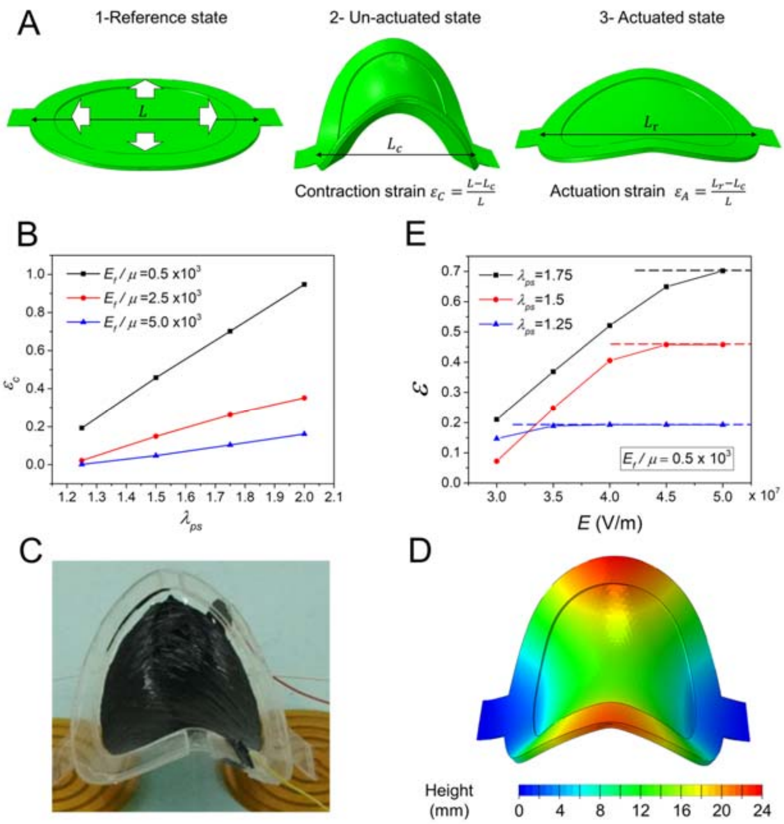

Fig. S4. Model simulation of the dielectric-elastomer actuator. (A) 1-Reference state with the pre-stretched dielectric-elastomer actuator (biaxially pre-stretched ratio λ_{ps}); 2-Rest state: when releasing the pre-stretching, the dielectric-elastomer actuator generates a contraction strain ε_C ; 3-Actuated state: when applying a voltage, the actuator undergoes large shape deformations and generates a corresponding actuation strain ε_A. (B) Relationship between ε_C and λ_{ps} under different frame vs. dielectric-elastomer modulus ratio E_f / μ (μ =0.2MPa). (C) Experimental deformation of the actuator ($E_f = 4GPa, \mu = 0.2MPa$) with contraction strain ε_C =0.21. (D) Simulated deformation of the actuator with the contraction strain ε_C =0.21. The contour indicates the height distribution in the vertical direction. (E) Relationship between actuation strain ε_A and applied electrical field E under different λ_{ps} and fixed $E_f / \mu = 0.5\times10^3$. Dashed lines represent the maximum actuation strain for the flattened frames (as in Fig. S4A1).

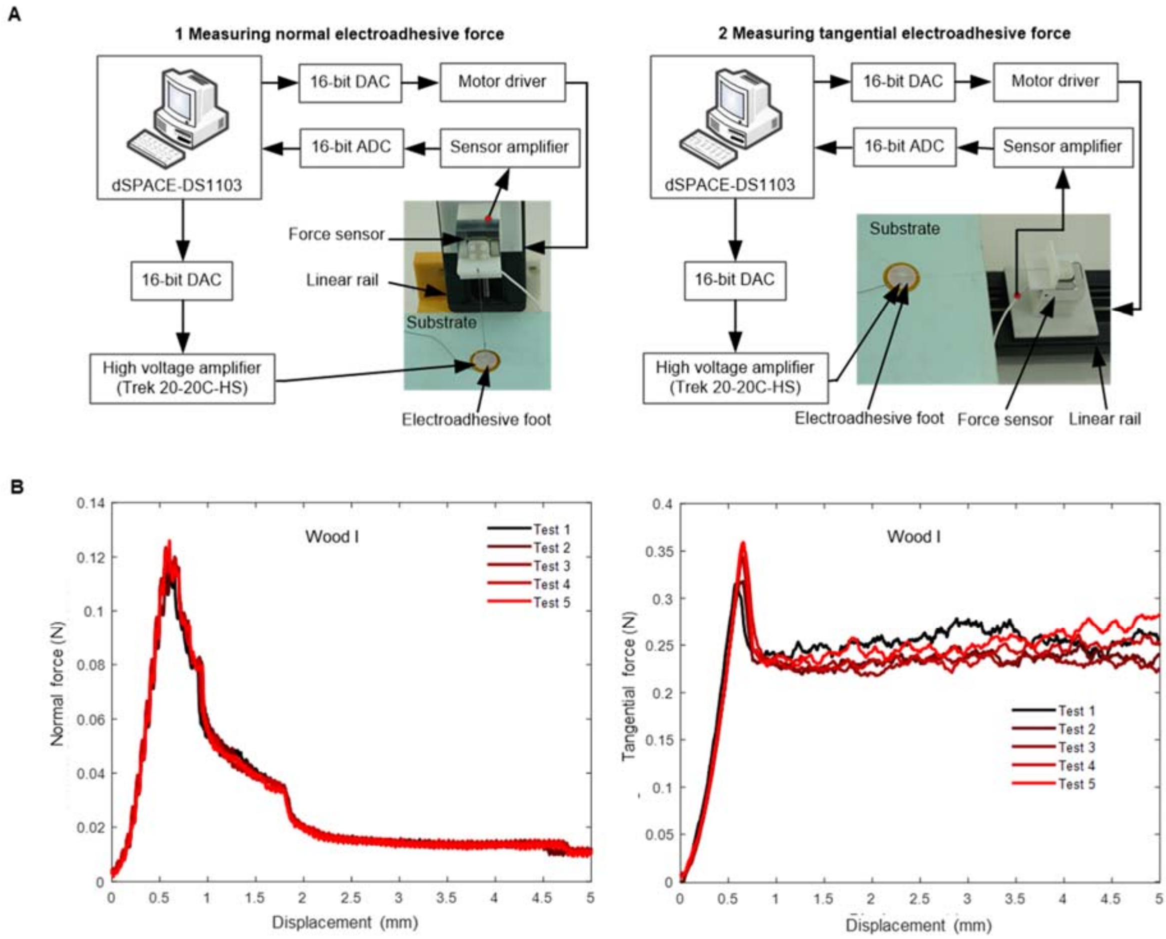

Fig. S5. Experimental setup for the electroadhesion measurement. A high-voltage amplifier (TREK 20/20C-HS) with a fixed gain of 2000 output actuation voltage for the electroadhesive foot. A three-dimension force sensor (Transform, K3D40) recorded the elelctroadhesion force of the foot. A linear rail was adopted to provide the horizontal or vertical movement. A dSPACE-DS1103 board generated the control signals for the high-voltage amplifier and the linear tail, and simultaneously recorded the electroadhesion force of the foot by the force sensor. The sampling time of the dSPACE-DS1103 board was set to be 1ms.

(A1) The measurement process of the normal electroadhesion force could be described as i) at the beginning, the foot was contacted with the substrate that was fixed by a substrate holder; ii) the foot was connected to the force sensor by a string (diameter=0.25mm); iii) using the high-voltage amplifier to apply a step voltage to the foot; iv) after 2 seconds, activating the linear rail to pull the foot with a speed of 1mm/s along normal direction, and the force senor recorded the tension on the string; v) when the displacement reached 5mm, the measurement was stopped; vi) we changed the amplitude of the step voltage and repeated the measurement process.

(A2) To measure the tangential electroadhesion force, the measuring method was same as measuring the normal force, while the only difference was that the linear rail needed to provide a tangential movement for the foot instead of the normal movement.

(B) One example of the force-displacement curves of the measured normal and tangential electroadhesion forces on the wood I substrate when 5kV was applied on the foot (each plot includes five times measurements). It can be seen that the normal electroadhesion force decreases to zero with the increase of the moving displacement because it is inverse proportional to square of the gap distance between the electroadhesive foot and the substrate. However, the tangential electroadhesion force doesn't decrease to zero because the electroadhesive foot remains in contact with the substrate throughout the tangential electroadhesion force measurement. Therefore, different from the normal one, the tangential electroadhesion force is usually difficult to quantify, which is greatly influenced by the applied voltage (*36, 49-53)*, substrate surface and initial preloading force on the foot. In this work, the maximum measured forces on different substrates under different applied voltages are, respectively, taken as the recorded value of the electroadhesion forces in Fig. 2B.

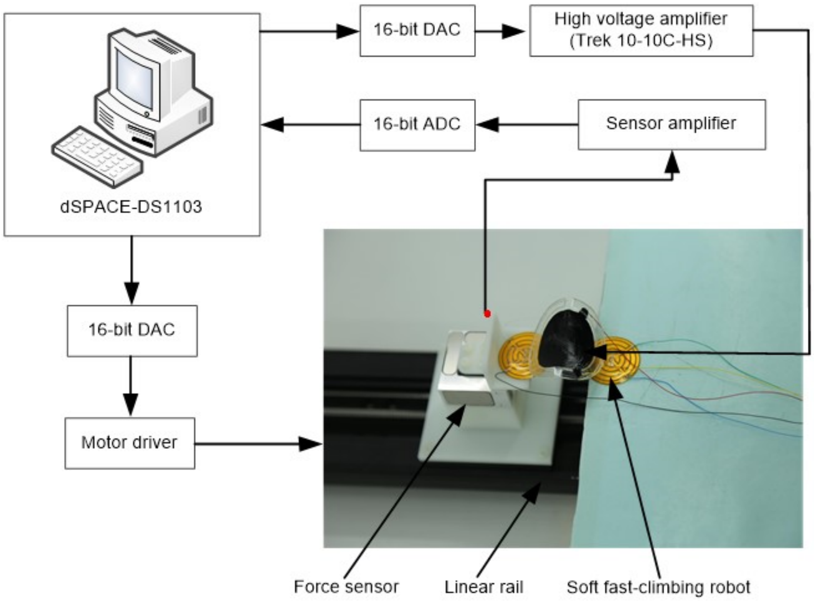

Fig. S6. Experimental setup for the blocking force measurement. The linear rail was adopted to provide the horizontal movement. A high-voltage amplifier (TREK 10/10C-HS) with a fixed gain of 1000 outputted driven voltage for the dielectric-elastomer actuator. A dSPACE-DS1103 board generated the control signals for the high-voltage amplifier and the linear rail and simultaneously recorded the force signals from the force sensor (Transform, K3D40). The sampling time of the dSPACE-DS1103 board was set to be 1ms.

To measure the blocking force, we fixed one foot onto a plate and connected the other one to the force sensor that was installed on the linear rail. The measurement process included five steps. i) Keeping the soft robot at the rest state, the blocking force equaled to zero. ii) Applying a step voltage to the dielectric-elastomer actuator. iii) After two seconds, the linear rail started to generate a horizontal movement with a speed of 1 mm/s. iv) when the moving displacement reached 10 mm, the measurement process stopped. v) We repeated the measurement with different amplitude of the step voltage.

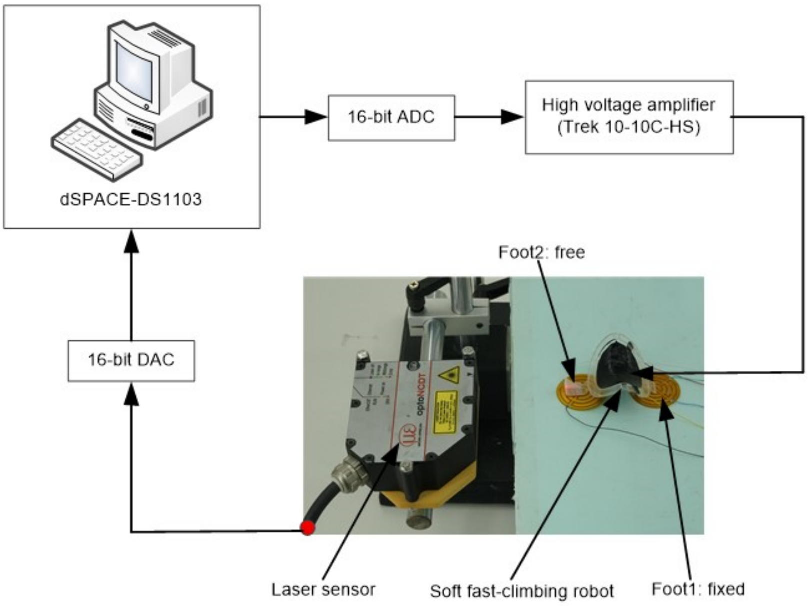

Fig. S7. Experimental setup for the extension measurement. A high voltage amplifier (TREK 10/10C-HS) with a fixed gain of 1000 outputted driven voltages for the dielectric-elastomer actuator. A laser sensor (Micro-Epsilon ILD2300-100) measured the extension length of the actuator. A dSPACE-DS1103 board generated the control signal for the high voltage amplifier and recorded the real-time displacements from the laser sensor. The sampling time was 1ms. A baffle plate was adhered to the free foot of the soft robot to provide convenience for laser sensors measuring.

To measure the extension length of the dielectric-elastomer actuator, four steps were involved. i) We fixed one foot onto a plate and kept the other one free of motion. ii) Sinusoidal voltage was applied to the dielectric-elastomer actuator. iii) When the actuation periods reached at least 20 (it should be noted that when the frequency was below 5Hz, the actuation periods was 20 and when the frequency was larger than 5Hz, the actuation time was set to be 5 seconds), the measurement stopped. iv) We repeated the measurement with different amplitude and frequency of the sinusoidal voltage.

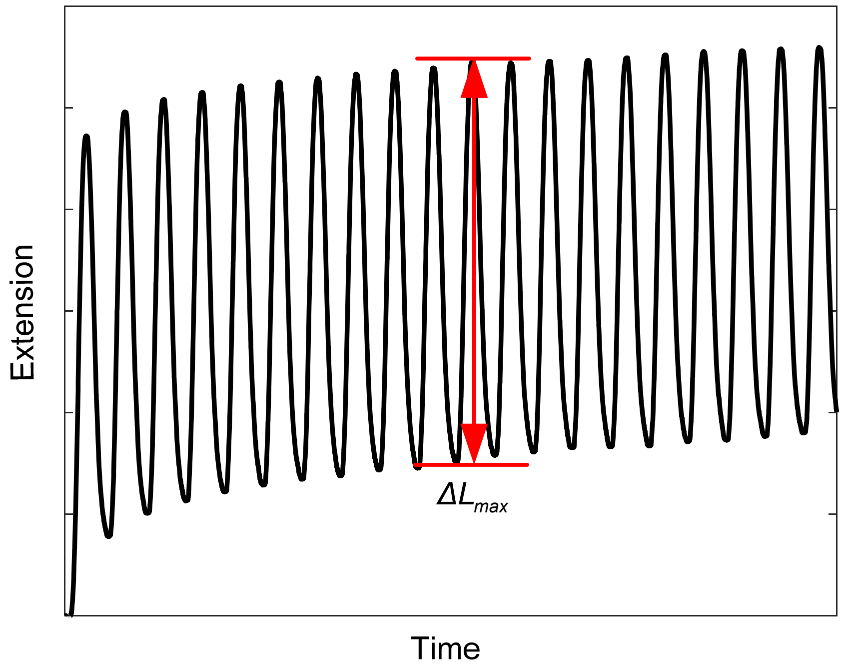

Fig. S8. Maximum extension length calculated in one actuation cycle. We observed that there was a drift phenomenon of the output displacement due to the viscoelasticity of the dielectric-elastomer actuator. In this study, the maximum extension length $\Delta L_{\max}$ was calculated as the deviation between the maximum and minimum extension in one cycle. We found that the maximum extension length was approximately constant without suffering from the drift except the first cycle.

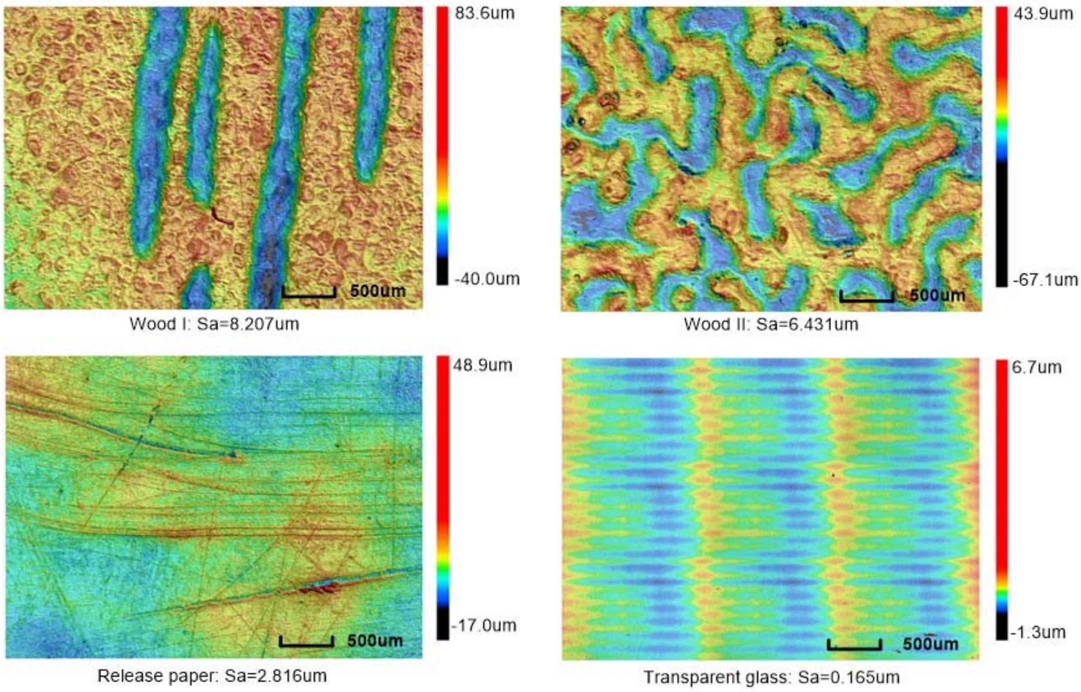

Fig. S9. The surface topography of different substrates. Both the wood I and wood II are particle board (Xuzhou Weibang Furniture Co. Ltd., China) with a thickness of 20mm, and the mainly difference is the texture of the surface. The release paper (8LK, Lintec Corp., Japan) is with thickness of 0.1mm. The transparent glass (Suzhou Fangyuan Glass Co. Ltd., China) is a toughened glass with a thickness of 5mm.

We use a 3D Laser Scanning Confocal Microscope (VK-X200, Keyence Corp., Japan) to measure the surface topography. The surface roughness (denoted as *Sa*) of four substrates are then characterized by the arithmetical average height through the following three steps.

i), We randomly choose an area in the XY plane, and the microscopy VK-X200 is used to measure the height $Z(x, y)$ of every point in selected area.

ii), We define an average plane A of the measured area with a height of h. The height h can then be solved by:

$$\iint_A \left[Z(x,y) - h \right] dxdy = 0$$

With the defined average plane (i.e., the zero plane for the next analysis), we can obtain the height information of the surface as indicated by the height distribution in the vertical direction in the figures.

iii), We calculate the arithmetical average height by:

$$Sa=\frac{\iint_A |Z(x,y)\text{-}h| dxdy}{\iint_A dxdy}$$

Therefore, the surface roughness (*Sa*) of the wood I, wood II, release paper and transparent glass can be calculated as 8.207um, 6.431um, 2.816um and 0.165um, respectively.

Table. S1 The currently available soft crawling robots and soft climbing robots

Soft Robots	Actuation	Structure	Maximum speed	Reciprocated Crawling	Wall Climbing	Untethered/ Tethered
Shepherd, 2011[54]	Pneumatic	Quadruped	0.2 BL/s (crawling) 0.03 BL/s (undulation)	No	No	Tethered
Drotman, 2017[55]	Pneumatic	Quadruped	0.13 BL/s (crawling)	No	No	Tethered
Verma, 2018[44]	Pneumatic	Tube climer	~0.1BL/s (tube climbing)	Yes	Only in tube	Tethered
Rafsanjani, 2018[34]	Pneumatic	Snake	0.04 BL/s (crawling)	No	No	Untethered
Wang,2018[32]	Liquid-crystal elastomer	Inchworm	0.001 BL/s (crawling)	Yes	No	Tethered
Wang, 2014[56]	Shape memory alloy	Inchworm	0.02 BL/s (crawling) N/A (turning)	No	No	Tethered
Umedachi, 2016[33]	Shape memory alloy	Inchworm	0.025 BL/s (crawling)	No	No	Tethered
	Motor-tendon	Inchworm	0.56 BL/s (crawling)	No	No	Tethered
Pei, 2002[57]	Dielectric-elastomer	Hexapod	0.35 BL/s (walking)	No	No	Tethered
Duduta, 2017[58]	Dielectric-elastomer	4-foot	1.03 BL/s(crawling)	No	No	Tethered
Qin, 2018[59]	Dielectric-elastomer	Inchworm	0.038 BL/s (crawling)	No	No	Tethered
Cao,2018[35]	Dielectric-elastomer	Inchworm	0.02BL/s (crawling) N/A (turning)	Yes	No	Untethered
This work	Dielectric-elastomer	2-foot or 4-foot	0.75BL/s (wall climbing) 1.04 BL/s (crawling) 62.79 °/s (turning)	Yes	Yes	Tethered

Remark: BL/s in the table represents body length per second.

Supplementary Movies

Movie S1 (.MP4 formant) Climbing experiments without payload

Movie S2 (.MP4 formant) Climbing experiments with a 10g payload

Movie S3 (.MP4 formant) Crawling experiments

Movie S4 (.MP4 formant) Turning experiments

Movie S5 (.MP4 formant) Video-recording while climbing a vertical tunnel

Movie S6 (.MP4 formant) Confined space navigation experiment

Movie S7 (.MP4 formant) Labyrinth trajectory tracking experiment

Movie S8 (.MP4 formant) Reciprocated crawl on the glass plane